Efficient Real-Time Time-Dependent Density Functional Theory Method and its Application to a Collision of an Ion with a 2D Material

Zhi Wang, Shu-Shen Li, and Lin-Wang Wang

Phys. Rev. Lett. **114**, 063004 — Published 13 February 2015

DOI: 10.1103/PhysRevLett.114.063004

Efficient real-time time-dependent DFT method and its application to a collision of an ion with a 2D material

Zhi Wang[1,2], Shu-Shen Li[1], Lin-Wang Wang[2*]

[1]State Key Laboratory for Superlattices and Microstructures, Institute of Semiconductors, Chinese Academy of Sciences, P.O. Box 912, Beijing 100083, China

[2]Material Sciences Division, Lawrence Berkeley National Laboratory, Berkeley, California 94720, USA

ABSTRACT

We have developed an efficient real-time time-dependent density functional theory (TDDFT) method that can increase the effective time step from <1 attosecond in traditional methods to 0.1~0.5 femtosecond. With this algorithm, the TDDFT simulation can have comparable speed to the Born-Oppenheimer (BO) ab initio molecular dynamics (MD). As an application, we simulated the process of an energetic Cl particle colliding onto a monolayer of $MoSe_2$. Our simulations show a significant energy transfer from the kinetic energy of the Cl particle to the electronic energy of $MoSe_2$, and the result of TDDFT is very different from that of BO MD simulations.

Time-dependent density functional theory (TDDFT) has been widely used from optical excitation [1-4] to ion-material collisions [5-7]. For optical excitation, the TD-DFT can be solved under linear perturbation theory [8] using Casida formalism. In Ref.[9], the phonon dynamic has also been incorporated into the TD-DFT in a perturbation theory. On the other hand, for many problems, direct real-time evolution of the Schrodinger's equation is necessary, e.g., to study nonlinear optical response [10], ultrafast magnetic dynamics [11], or to study an ion collision with a substrate [6,12-14]. TD-DFT can also be viewed as belonging to the general non-adiabatic molecular dynamic (NA-MD) [15,16]. In NA-MD, the electron wave function follows the time dependent Schrodinger equation, while the nuclear movement follows the classical Newton's law. The direct NA-MD without introducing the energy surface hopping [17], or wave function collapsing [18] is also called Ehrenfest dynamics [19]. Compared to the adiabatic Born-Oppenheimer ab initio molecular dynamics (BO-MD), the NA-MD can be used to study problems where the electronic states are excited during the dynamics process, e.g., the carrier cooling [20], carrier transport [21,22] and charge transfer induced chemical reaction [23]. While extremely powerful, so far the real-time TD-DFT suffers from its extremely high computational cost. The time step it can use is typically around 1 attosecond (as), compared to 1 femtosecond (fs) time step in BO-MD. In this work, we present a new algorithm which can increase the effective time step to 0.1~0.5 fs, hence makes it comparable to the BO-MD simulations.

Many algorithms have been developed in literature to evolve the wave functions directly starting from the fundamental formula $\psi_i(t+dt) = e^{-iHdt}\psi_i(t)$. Taylor expansion, split operator [24, 25], and Lanczos methods [26] have been used to approximate e^{-iHdt}. But all these approximations require $|Hdt| << 1$ for accurate evaluation of this operator. However, since the energy spectrum width of H, especially under the flexible plane wave basis set, can be rather large (e.g., 400 eV), this results in dt < 10^{-3} fs. Here, we will follow the formalism often used in quantum chemistry, expanding $\psi_i(t)$ by the adiabatic eigen states $\varphi_l(t)$. Under the TD-DFT formalism, a set of occupied single particle states $\{\psi_i(t)\}$ will be calculated following time dependent Schrodinger's equation:

$$i\partial\psi_i(t)/\partial t = H(t, R_j(t), \rho(t))\psi_i(t), \qquad \rho(t) = \sum_i |\psi_i(t)|^2 \tag{1}$$

i=1,M is the index of the occupied states, and M is the number of electron. The instantaneous exchange-correlation functional approximations will he used in the $H(t, R_j(t), \rho(t))$ expression and external stimulation (e.g., external photon potential) can also be included in H. The nuclear positions $R_j(t)$ will follow

$$M_j d^2 R_j(t)/dt^2 = F_j(t) \tag{2}$$

$F_j(t)$ is the ab initio force on the j-th nuclear with mass M_j calculated from the DFT total energy $E(\{R_j(t)\}, \{\psi_i(t)\})$ as $F_j = -\partial E(\{R_j\}, \{\psi_i\})/\partial R_j$ (with a formula and implementation similar to that of the Hellmann-Feynman theory). The Eq.(1), (2) constitute an Ehrenfest dynamics [19].

To integrate Eq.(1), we will expand $\psi_i(t)$ in terms of the adiabatic eigen states $\varphi_l(t)$:

$$\psi_i(t) = \sum_i C_{i,l}(t)\varphi_l(t) \tag{3}$$

and here ($H(t) \equiv H(t, R_j(t), \rho(t))$)

$$H(t)\varphi_l(t) = \varepsilon_l(t)\varphi_l(t) \tag{4}$$

Now, plug Eq.(3), (4) into Eq.(1), we have:

$$\dot{C}_{i,l}(t) = -i\varepsilon_l(t)C_{i,l}(t) - \sum_k C_{i,k}(t)V_{lk}(t) \tag{5}$$

where

$$V_{lk}(t) = \left\langle \varphi_l(t) \middle| \partial\varphi_k(t)/\partial t \right\rangle \tag{6}$$

Due to the fact that $\varepsilon_l(t)$ appears explicitly in the diagonal term in Eq.(5), the dt used to evolve Eq.(5) will no longer be limited by the energy spectrum width of H. In practice, however, the dt used to integrate Eq.(5) can still be rather small due to the off diagonal term $V_{lk}(t)$, which describes the coupling between adiabatic states l and k. The $V_{lk}(t)$ can have very sharp peak with time, especially when coupling between l and k are weak [27]. This difficulty however is in a sense artificial due to the use of $\varphi_l(t)$ which can change its identity suddenly when two states anticross each other in energy (hence $\partial\varphi_k(t)/\partial t$ in Eq.(6) becomes extremely large). In [27], we have developed an algorithm to overcome this problem. Under this algorithm, during the time interval $[t_1, t_2]$, we can use $\varphi_l(t_1)$ as the basis to represent the Hamiltonian as a matrix, then every element of this matrix within $[t_1, t_2]$ can be approximated as

$$H(t) = H(t_1) + (t - t_1)/(t_2 - t_1) \times (H(t_2) - H(t_1)) \tag{7}$$

In order to obtain the two matrices H(t_1) and H(t_2), all we need to have are $\{\varepsilon_l(t_1), \varphi_l(t_1)\}$ and $\{\varepsilon_l(t_2), \varphi_l(t_2)\}$. It has been shown that [27], for a typical carrier dynamics problem, Eq.(7) holds very well for $\Delta t = t_2 - t_1 \le 0.5$ fs. Now, to integrate the Eq.(5), (6) from t_1 to t_2, an small dt (< attosecond) is used. However, within the [t_1,t_2] interval, instead of solving {φ_l(t)} from the original Hamiltonian (Eq.(4)) for every dt step, we solve {φ_l(t)} by diagonalizing the matrix of Eq.(7), and representing {φ_l(t)} with {φ_l(t_1)}. This requires the diagonalizing of a NxN H_{ij}(t) matrix from Eq.(7) for every dt step, where N is the number of adiabatic state included in Eq.(3). A major saving comes when we truncate the number N, so it is significantly smaller than the original number of plane wave basis function in Eq.(1) and Eq.(4) (which can be a thousand time larger than N). As a result, the computational time on the integration of Eq.(5) and (6) is negligible compared to the time for solving Eq.(4). The actual choice of N might depend on the problems. However, for most cases, a few eV above the ground state's highest occupied adiabatic state might be good enough. For the problems to be studied later in this paper, we have used N=2M, where M is the number of occupied orbitals. More technical details can be found in

Ref.[27] and in the supplementary material (SM). Note that, if needed, a further speed up is possible by not diagonalizing the matrix $H_{ij}(t)$ at each dt step within $[t_1,t_2]$, but to integrate $\psi_i(t)$ from Eq.(1) under the fixed basis set of $\{\varphi_l(t_1)\}$ and the $H_{ij}(t)$ of Eq.(7), and only change the basis set from $\{\varphi_l(t_1)\}$ to $\{\varphi_l(t_2)\}$ at $t=t_2$.

The above scheme has been worked out in Ref.[27]. However in Ref.[27] only one carrier wave functions are integrated with time, and the nuclear force is provided by classical force fields. Here, we will consider all occupied states $\psi_i(t)$ and use the DFT atomic forces calculated from $\psi_i(t)$ for nuclei dynamics. There is however one problem needs to be solved. When using Eq.(7), we need to know Hamiltonian $H(t_2)$ at time t_1. This requires us to know $\rho(t_2)$ while at $t=t_1$. We have used an iterative leapfrog method to solve this problem. More specifically, at $t=t_1$, we first estimate $\rho(t_2)$ (e.g., using linear extrapolation from previous steps), then get $H(t_2)$ and $\{\varphi_i(t_2), \varepsilon_i(t_2)\}$. We will use this to carry out Eq.(5)-(7), that will yield a new $\rho'(t_2)$. Then a mixed charge $\rho''(t_2)$ from $\rho(t_2)$ and $\rho'(t_2)$ (e.g., with the Kerker algorithm [28]) will be used in next loop. This will be repeated until $\rho'(t_2)$ and $\rho(t_2)$ are close to each other. In practice, we found that about 4 iterations are needed to get a well converged result. For the nuclear dynamics, we use the Verlet algorithm, hence while the electronic energies and atomic forces are evaluated at t_1,t_2 points, the velocities are evaluated at $(t_1+t_2)/2$ point. Thus, at t_1, we know $F_j(t_1)$, hence know $V_j((t_1+t_2)/2)$, then $R_j(t_2)$. The total energy can be evaluated at $(t_1+t_2)/2$, with the electronic energy at that point being the average of the values at t_1 and t_2. A good way to test the accuracy of the Ehrenfest dynamics is to check the total energy conservation during the simulation.

To test the above algorithm, we have first applied it to a few simple systems. Norm conserving pseudopotentials are used with plane wave basis set in the original Hamiltonian. PBE [29] generalized gradient approximation functional is used. The ground states $\{\varphi_l(t)\}$ at each Δt step $(t_1,t_2,..)$ are calculated by the conjugate gradient method as implemented in PEtot code [30]. The evolution of Eq.(5) for different "i" in $C_{i,l}(t)$ can be carried out with different processors, results in high parallelization to carry out Eq.(5).

The first test system is an 8 atom cell CdSe with only Γ point. It has 72 electrons in total, we have used 72 adiabatic states (note each state can be occupied by 2 electrons). The result of Eq.(5)-(7) with $\Delta t=0.2$ fs and the one integrated from a simple direct integration: $\psi_i(t+dt)=\psi_i(t)-idtH(t)\psi_i(t)$ with $dt=10^{-5}$ fs are shown in Fig.1S and Fig.2S of the supplemental materials. The difference of these two simulations is extremely small and the remaining small error comes from the non-convergence of the direct integration method regard to dt.

For a second test, we have calculated the light absorption spectrum of a 50 atom Au cluster using the new real time TDDFT method, and compared the result with the linear perturbation TDDFT method (using PWscf code [31]). The excellent agreement is shown in Fig.3S. The third test system is a 3x3x3 Aluminum cluster (of 4 atom face center cubic cell, hence with 108 Al atoms). An initial nuclei velocity is set according to 300K temperature, and an initial carrier excitation from one valence state to

one conduction band state is used as shown in Fig.4S. This problem mimics a hot carrier cooling process in a metal cluster, a very important topic in plasmonic harvest of hot carriers [32, 33]. The system contains 324 electrons. Here we have used 324 adiabatic states (2 electrons per state) with roughly half to be occupied. In Fig.5S, the total energy is shown together with the kinetic energy and potential energy (the DFT energy). As can be seen the total energy is well conserved, indicating the overall high accuracy of the Ehrenfest dynamics. We do note that, to simulate a hot carrier cooling accurately, one does need to include the beyond Ehrenfest dynamics methods [17, 18, 27].

Finally we have applied TD-DFT method on a Chlorine atom (or ion) colliding to a monolayer of $MoSe_2$. Transition-metal dichalcogenides MeX_2, where Me stands for transition metals (Mo, W, Ti, etc.) and X for chalcogens (S, Se, Te), are important new 2D materials with potential usage in beyond CMOS electronic devices, or renewable energy applications [34-36]. One possible way to dope the system is to replace one chalcogen by one Cl or Br [37]. Such doping process can be done in many different ways, but a standard way in the electronic industry is via the ion implantation, where an ion beam directly collides with the substrate [38]. Ions and graphene collision has been simulated with TD-DFT methods before [12-14].

The system studied is shown in Fig.1. Initially, Cl^- ion (or neutral Cl atom) is placed 5 Å away from a monolayer $MoSe_2$, but is having a perpendicular 0.5 Å/fs velocity which corresponds to a kinetic energy of 460eV. To avoid the possible small variation in the result due to random thermo movement, we have set the initial temperature to zero (although an initial room temperature would only give a negligible small difference). A 28 atoms (including Cl) 3x3 $MoSe_2$ superlattice is built with periodic boundary conditions, sampled with Γ point only. The vertical direction dimension is 10 Å. 30 Ryds plane wave cutoff is used. 170 adiabatic states (2 electrons per state) are used, and there are 170 valence electrons for the Cl^- ion case. We have simulated 7 projectiles all located near the center of the hexagonal ring, as indicated by the red points in Fig.1(b). The time for the ion to travel through this system is about 26 fs, thus we have only simulated 26 fs, although much longer time simulation is possible. The Δt ($=t_2-t_1$) we used is 0.1 fs. It costs about 20 hours on 128 processors to simulate one 26 fs projectile. We have also considered both Cl^- ion and neutral Cl atom collisions in order to compare with BO-MD results, since in BO-MD, there is no easy way to simulate Cl^- ion collision (the additional electron will occupy the $MoSe_2$ conduction band state, instead of the Cl^- state).

The projectile at the exact hexagonal central point is shown in Fig.2. In this case, the Cl ion (or atom) passes through the $MoSe_2$ without destroying it. Three energies are shown with time: the $MoSe_2$ nuclear kinetic energy (green), the Cl nuclear kinetic energy (red) and the total electronic energy of the system (blue, this is the DFT energy at a given point). The sum of these three energies is the total energy of this system, which is a straight line (thus not shown). We first see that, the Cl^- and Cl results are rather similar, thus we will represent them with Cl in the following discussion. During the collision, the electronic system of the $MoSe_2$ takes 15~24eV from the kinetic energy of the Cl. Under BO-MD simulation, most of these electronic energies are given back to the Cl atom, thus at the end the Cl atom

only loses 1.63eV converting to the nuclear kinetic energy of $MoSe_2$. On the other hand, for TD-DFT simulation, 14eV kinetic energy is lost for Cl, which has been converted to the electronic excitation in the $MoSe_2$ system (which cannot be described by BO-MD). To better illustrate the kinetic energy loss and electron excitation in the TD-DFT simulation, we have shown in Fig.3 the electron occupation among the adiabatic density of states (DOS) (as defined by $\sum_{i=1,m}|C_{i,l}(t)|^2$ for each adiabatic state $\varphi_l(t)$) at 6 time steps during the collision process. We can see that, at the end of the collision, in the TD-DFT simulation, there are electron occupations in the conduction band (mostly in the partial DOS of $MoSe_2$), while in BO-MD, by construction, that is not allowed. These higher energy excitations account for the 14 eV kinetic energy loss. We note that in the electronic energy curve of Fig.2, there are three sharp peaks near 10fs, 13fs and 17fs, they all have a width of $\tau \approx 2fs$. These energy peaks are representations of the Hamiltonian changes, their 2 fs width corresponds to a Fourier periodicity of 4 fs, hence an energy $E = h\omega$ ~1eV, which coincides with the $MoSe_2$ band gap and the excitation energy shown in Fig.3. This means the Hamiltonian change induced by the Cl collision provides high frequency perturbation to excite the $MoSe_2$ system over its band gap. Finally, we note that there is no occupation near the upper end of the energy spectrum shown in Fig.3, which means the $\{\varphi_l(t)\}$ truncation we have used in Eq.(3) is adequate. Meanwhile, we find a charge transfer after the collision. While the Cl^- ion loses -0.36e after the collision, the neutral Cl atom only loses -0.01e charge. To describe such charge transfer more rigorously, one has to go beyond the Ehrenfest dynamics, describing the charge transfer as a probabilistic event [17, 18], not as a partial charge occupation in Cl ion as in the mean field theory Ehrenfest description. Nevertheless, the charge loss does explain why the Cl^- state has lowered its energy after the collision as shown in Fig.3(a).

For other projectiles not exactly at the center of the hexagon, their final Cl atoms will flight in slightly deflected directions and with different energy loss. This direction-energy relationship can be used experimentally to test the result of our simulation. We have fit the simulated flight-out Cl kinetic energy as a function of the angle of emergence θ and φ (as their definitions in Fig.1(c)) based on the 7 projectiles (Fig.1(b)) and the symmetry considerations:

$$T_{Cl}^{out} = T_0 - \alpha(1+\beta\cos 6\theta+\gamma\cos 3\theta\cos 6\theta)\varphi^2 \quad (8)$$

The resulting parameters of the three simulations (Cl^- with TDDFT, Cl with TDDFT and Cl with BO-MD) are shown in Table.1S. The kinetic energy loss $\Delta T_{Cl}=T_{Cl}^{in}-T_{Cl}^{out}$ of the Cl^- ion with TDDFT and the Cl atom with BO-MD are shown in Fig.4. Future experiments need to be carried out to verify our results.

Acknowledgement:

This work is supported by the Director, Office of Science, Office of Basic Energy Science, Materials Science and Engineering Division, of the U.S. Department of Energy under Contract No. DE-AC02-05CH11231, through the Material Theory program in Lawrence Berkeley National

Laboratory. Zhi Wang is supported by the China Scholarship Council. This work uses the resource of National Energy Research Scientific Computing center (NERSC).

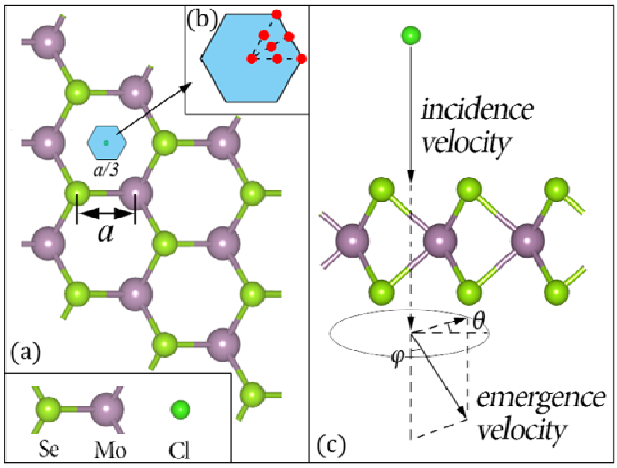

Fig. 1: (color online) The model of Cl-$MoSe_2$ collision. a is the horizontal distance between nearest neighbors, a=1.890 Å. The region of incidence has been colored blue in (a) and zoomed in (b). Red points in (b) show the initial positions of Cl. Scattering angles θ and φ are defined as shown in (c).

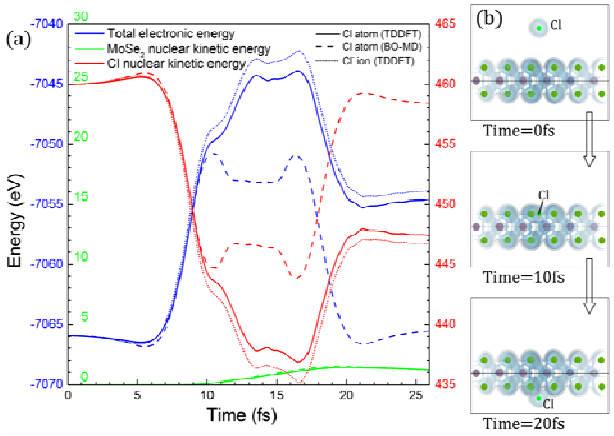

Fig. 2: (color online) (a) Electronic and nuclear kinetic energies during the central point penetration, and (b) the atom positions and charge density isosurfaces at 3 time steps.

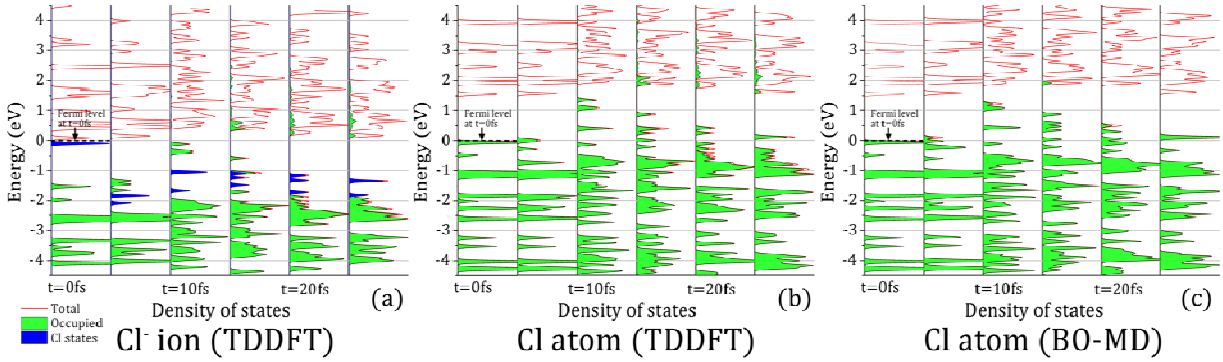

Fig. 3: (color online) Snapshots for density of states and occupations at 6 time steps, under different cases. Energy zero points are selected equal to the initial Fermi-energies. Only states near Fermi-energy are shown (-4.5eV to 4.5eV). Green, blue and red states are occupied adiabatic states, Cl occupied states, and unoccupied adiabatic state, respectively.

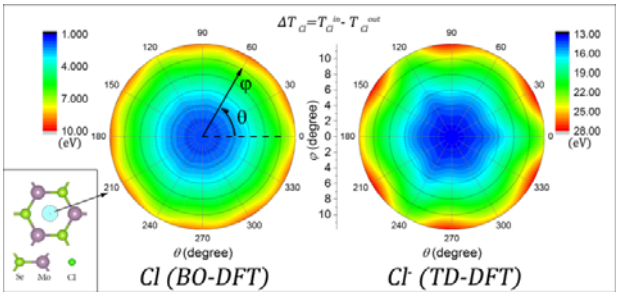

Fig. 4: (color online) Polar plots for projectile energy loss ΔT_{Cl} from Eq. (8) under different cases. From center to the peripheral, the φ changes from 0 degree to 12 degree. A diagrammatic sketch for the incidence region has been shown in left down corner.

[1] A. Tsolakidis, D. Sánchez-Portal, and R. M. Martin, Phys. Rev. B **66**, 235416 (2002)
[2] F. De Angelis, A. Tilocca, and A. Selloni, J. Am. Chem. Soc. **126**(46), 15024 (2004)
[3] J. L. Bingaman, C. L. Kohnhorst, G. A. Van Meter, B. A. McElroy, E. A. Rakowski, B. W. Caplins, T. A. Gutowski, C. J. Stromberg, C. E. Webster, and E. J. Heilweil, J. Phys. Chem. A **116**(27), 7261 (2012)
[4] P. Cudazzo, K. O. Ruotsalainen, C. J. Sahle, A. Al-Zein, H. Berger, E. Navarro-Moratalla, S. Huotari, M. Gatti, and A. Rubio, Phys. Rev. B **90**, 125125 (2014)
[5] V. U. Nazarov, J. M. Pitarke, C. S. Kim, and Y. Takada, Phys. Rev. B **71**, 121106(R) (2005)
[6] S. Bubin, Bin Wang, S. Pantelides, and K. Varga, Phys. Rev. B **85**, 235435 (2012)
[7] Matthew Baxter and Tom Kirchner, Phys. Rev. A **87**, 062507 (2013)
[8] ME Casida, in Recent Advances in Density Functional Methods, Part I, edited by DP Chong (World Scientific, Singapore, 1995), p. 155
[9] Vladimir U. Nazarov, Fahhad Alharbi, Timothy S. Fisher, and Sabre Kais, Phys. Rev. B **89**, 195423 (2014)
[10] Y. Takimoto, F.D. Vila, J.J. Rehr, J. Chem. Phys. **127**, 154114 (2007)
[11] G.P. Zhang, W. Hubuer, G. Lefkidis, Y. Bai, T.F. George, Nat. Phys. **5**, 499 (2009)
[12] Y. Miyamoto, Appl. Phys. Lett. **91**, 113120 (2007)
[13] A. V. Krasheninnikov, Y. Miyamoto, and D. Tománek, Phys. Rev. Lett. **99**, 016104 (2007)
[14] Y. Miyamoto, and Hong Zhang, Phys. Rev. B **77**, 161402(R) (2008)
[15] M. Born and J. R. Oppenheimer, Ann. Phys. **84**, 457 (1927)
[16] R. de L. Kronig, Band Spectra and Molecular Structure (Cambridge University Press, New York, 1930)
[17] J. C. Tully, J. Chem. Phys. **93**, 1061 (1990)
[18] J. Bedard-Hearn, R. E. Larsen, and B. J. Schwartz, J. Chem. Phys. **123**, 234106 (2005)
[19] J. B. Delos and W. R. Thorson, Phys. Rev. A **6**, 720 (1972)
[20] S. V. Kilina, D. S. Kilin, and O. V. Prezhdo, ACS Nano **3**, 93 (2009)
[21] J. Pittner and M. J. Pederzoli, Phys. Chem. A **115**, 11136 (2011)
[22] I. Tavernelli, B. F. E. Curchod, and U. Roethlisberger, Chem. Phys. **391**, 101 (2011)
[23] C. F. Craig, W. R. Duncan, and O. V. Prezhdo, Phys. Rev. Lett. **95**, 163001 (2005)
[24] M. Suzuki, J. Phys. Soc. Jpn. **61**, L3015 (1992)
[25] M. Suzuki and T. Yamauchi, J. Math. Phys. **34**, 4892 (1993)
[26] A. Castro, M.A.L. Marques, H. Appel, M. Oliveira, C.A. Rozzi, X. Andrade, F. Lorenzen, E.K.U Gross, A. Rubio, Physica Status Solidi B **243**, 2465 (2006)
[27] Junfeng Ren, N. Vukmirović, and L.W. Wang, Phys. Rev. B **87**, 205117 (2013)
[28] G. P. Kerker, Phys. Rev. B **23**, 3082 (1981)
[29] J. P. Perdew, K. Burke, and M. Ernzerhof, Phys. Rev. Lett. **77**, 3865 (1996)

[30] This method was originally developed by L. W. Wang and implemented in his plane-wave pseudopotential code PETOT while at the National Renewable Energy Laboratory

[31] P. Giannozzi, S. Baroni, N. Bonini, M. Calandra, R. Car, C. Cavazzoni, D. Ceresoli, G. L. Chiarotti, M. Cococcioni, I. Dabo, A. Dal Corso, S. Fabris, G. Fratesi, S. de Gironcoli, R. Gebauer, U. Gerstmann, C. Gougoussis, A. Kokalj, M. Lazzeri, L. Martin-Samos, N. Marzari, F. Mauri, R. Mazzarello, S. Paolini, A. Pasquarello, L. Paulatto, C. Sbraccia, S. Scandolo, G. Sclauzero, A. P. Seitsonen, A. Smogunov, P. Umari, R. M. Wentzcovitch, J.Phys.:Condens.Matter **21**, 395502 (2009), http://arxiv.org/abs/0906.2569

[32] Kaibiao Zhang and Hong Zhang, J. Phys. Chem. C **118**(1), 635 (2014)

[33] Hongping Xiang, Xu Zhang, Daniel Neuhauser, and Gang Lu, J. Phys. Chem. Lett. **5**(7), 1163 (2014)

[34] B. Radisavljevic, A. Radenovic, J. Brivio, V. Giacometti, and A. Kis, Nature Nanotech. **6**, 147 (2011)

[35] I. Popov, G. Seifert, and D. Tománek, Phys. Rev. Lett. **108**, 156802 (2012)

[36] M. Chhowalla, H. S. Shin, G. Eda, L.-J. Li, K. P. Loh, and H. Zhang, Nat. Chem. **5**, 263 (2013)

[37] A. Carvalho and A. H. Castro Neto, Phys. Rev. B **89**, 081406(R) (2014)

[38] Hannu-Pekka Komsa, J. Kotakoski, S. Kurasch, O. Lehtinen, U. Kaiser, and A. V. Krasheninnikov, Phys. Rev. Lett. **109**, 035503 (2012)